Numerical study on suppression of vortex-induced vibrations of box girder bridge section by aerodynamic countermeasures

M.W. Sarwar *, T. Ishihara

Department of Civil Engineering, School of Engineering, The University of Tokyo, 7-3-1 Hongo, Bunkyo-ku, Tokyo 113-8656, Japan

ABSTRACT

This paper investigates the mechanism of reduction in the amplitude of vortex-induced vibrations for a box girder bridge section in the presence of aerodynamic countermeasures using 3D LES turbulence model. Being the basic configuration for the bridge section, the aeroelastic instability of rectangular section with an aspect ratio of 4 is investigated in heaving mode under smooth flow conditions and the wake characteristics are examined. Thereafter flow around box girder section having width to depth ratio of 3.81 in the presence of aerodynamic countermeasures is analyzed and the effect of these countermeasures on the unsteady lift forces is evaluated using forced oscillation simulations. Then response of the box girder section in the presence of such aerodynamic countermeasures is investigated by conducting the free oscillation simulations, and the predicted amplitudes of vibration are compared with the experimental results. Flow visualization is employed to clarify and understand the modified flow characteristics around bridge section in the presence of aerodynamic countermeasures resulting in a reduced amplitude of vibration. Further a method based on forced oscillations to identify the reduced velocity corresponding to the maximum amplitude of vibration is proposed.

© 2010 Elsevier Ltd. All rights reserved.

1. Introduction

Safety of long span bridges against wind loads is of primary concern during the design process. The wind-induced phenomena, particularly vortex-induced vibrations are often critical for safety and serviceability of long span bridges. Since selection of a bridge deck configuration depends on many factors such as structural and economical advantages, the basic deck shape does not necessarily have optimal aerodynamic efficiency. As a consequence, long span bridges are often subjected to vortex-induced vibrations, examples of which are Trans-Tokyo Bay Bridge and Storebælt Suspension Bridge. Different types of aerodynamic vibration control measures are often tested experimentally to find the most suitable vibration control measure. However, testing of such countermeasures is done on a case-by-case basis, e.g., fairings, double flaps and skirt were examined for Trans-Tokyo Bay Bridge (Fujino, 2003) and guide vanes were found suitable for Storebælt Suspension Bridge (Larsen et al., 2000). Efficiency of such countermeasures is found dependent on the geometrical configuration of bridge sections. Therefore, a measure suitable for one bridge section may show adverse effects in another case (Fujino and Yoshida, 2002). In addition, these experimental studies lack information on the vibration control mechanism of such aerodynamic countermeasures and therefore do not provide any guidance to select a countermeasure for other bridge sections experiencing similar problem.

Since the geometrical configuration of the bridge sections is generally based on the elongated rectangular cross-sections, a number of experimental investigations on the aerodynamic and aeroelastic properties of rectangular sections with aspect ratios closer to that of the bridge sections can be found in the literature (Washizu et al., 1978; Nakamura and Mizota, 1975; Komatsu and Kobayashi, 1980; Matsumoto, 1996; Matsumoto et al., 1994, 1996). The numerical modeling of fluid–structure interaction (FSI) is considered as a powerful tool to investigate the wind induced vibrations for its flexibility over traditional wind tunnel. A comprehensive research on the numerical modeling of the FSI of rectangular section is presented by Tamura and Itoh (1997) and Tamura (1999). These studies have shown detailed investigation on the free oscillations of rectangular sections of width to depth ratio of 2 using direct numerical simulation (DNS) and large eddy simulation (LES) turbulence model respectively. These studies introduced a transformation of the governing equations to the generalized coordinates in order to simulate the moving boundary conditions involved in FSI problems. The predicted free oscillation amplitudes were found in good agreement with the experimental results. Later Shimada and Ishihara (1999) and Shimada (2000) approached the FSI problem using the modified κ–ε model to predict the aeroelastic behavior of rectangular sections with width to depth ratios of 2 and 4. The simulated results compared well with the experimental observations for both the motion-induced and vortex-induced vibrations.

---

* Corresponding author. Tel.: +81 35 841 1145; fax: +81 35 841 1147.
E-mail address: sarwar@bridge.t.u-tokyo.ac.jp (M.W. Sarwar).

In the field of computational bridge engineering, the fluid structure interaction has been the main focus of many researchers and the major numerical approaches in this field include discrete vortex method (DVM), Reynolds average Navier–Stokes (RANS) model and large eddy simulations (LES). Many studies have successfully employed the grid free discrete vortex method for solving the flow around oscillating bridge sections to predict the flutter critical velocity (Larsen and Walther, 1998; Morgenthal, 2005; Larsen, 2006; Taylor and Vezza, 1999, 2009). Applications of DVM to predict the vortex-induced vibrations of Great Belt East Bridge are made by Morgenthal (2000) and Frandsen (1999). The lock-in phenomenon was clearly identified and impact of damping on the amplitude of vibration was pursued by Morgenthal (2000), but this study lacked the support of experimental or observation data. Whereas Frandsen (1999) showed fairly good agreement between the simulated amplitude of vibration and the field observations. DVM is widely used due to its significant benefits in terms of efficiency but it requires careful selection of "various parameters, such as core radius, defining the maximum circulation, and position of surface vorticity to be released from the bridge surface (Frandsen, 2004)". On the other hand, Larsen (2006) has applied RANS based k–ω SST method to simulate the unsteady forces and considerable discrepancy was found with regard to the onset velocity of flutter. The investigations on the vortex-induced vibrations of a Seohae bridge section using RANS approach are reported by Lee et al. (1997). A combination of a 2D fluid simulation and 3D structural model was used to predict the amplitude of vibration as an indirect verification of vortex loading. However, according to Bruno and Khris (2003), "This approach clearly does not permit any conclusions to be drawn on the reliability of the statistical approach". An other example of RANS application to simulate the vortex-induced vibrations of Kessock Bridge is conducted by Owena and Hargreavesa (2007). A relatively small amplitude was obtained at a low wind velocity compared to the experimental observations. Recently Sarwar et al. (2008) utilized the 3D large eddy simulation for determining the flutter characteristics of a box girder section and has shown good agreement between the experimental and numerical unsteady force characteristics.

This study aims to provide comprehensive investigations on the performance of 3D LES and to clarify the mechanism of reduction in amplitude of vortex-induced vibrations of a box girder bridge section by the aerodynamic countermeasures. First the aeroelastic instability of a rectangular section with aspect ratio close to the box girder section is investigated. Then influence of the aerodynamic countermeasures on the unsteady forces acting on the box girder section is analyzed, and a method based on the forced oscillation simulation is proposed to efficiently predict reduced velocity resulting in a maximum amplitude of vibration. Finally flow visualization is employed to examine the flow characteristics around box girder section and the mechanism of reduction in oscillation amplitude in the presence of the aerodynamic countermeasures is clarified.

2. Numerical model

2.1. Governing equations

The governing equations of the fluid domain are the filtered Navier–Stokes equations for constant density (incompressible) flow as follows:

$$\frac{\partial \rho \bar{u}_i}{\partial x_i} = 0; \quad \frac{\partial}{\partial t}(\rho \bar{u}_i) + \frac{\partial}{\partial x_j}(\rho \bar{u}_i \bar{u}_j) = \frac{\partial}{\partial x_j}\left(\mu \frac{\partial \bar{u}_i}{\partial x_j}\right) - \frac{\partial \bar{p}}{\partial x_i} - \frac{\partial \tau_{ij}}{\partial x_j} \quad (1)$$

where $\bar{u}_j$ is the filtered mean velocity, $\bar{p}$ is the filtered pressure and τ_{ij} is the subgrid scale stress that is modeled as follows:

$$\tau_{ij} = -2\mu_t \bar{S}_{ij} + \frac{1}{3}\tau_{kk}\delta_{ij}; \quad \bar{S}_{ij} = \frac{1}{2}\left(\frac{\partial \bar{u}_i}{\partial x_j} + \frac{\partial \bar{u}_j}{\partial x_i}\right) \quad (2)$$

where $\bar{S}_{ij}$ is the strain rate tensor of the resolved field and μ_t is the subgrid-scale eddy viscosity that is modeled (Smagorinsky, 1963) as follows:

$$\mu_t = \rho L_s^2 |\bar{S}| = \rho L_s \sqrt{2\bar{S}_{ij}\bar{S}_{ij}}; \quad L_s = \min(k\delta, C_s V^{1/3}) \quad (3)$$

where L_s is Smagorinsky length scale that depends upon von Kármán constant (k), distance to the closest wall (δ), Smagorinsky constant (C_s) and the volume of the computational cell (V). Conventionally a value of 0.1 is used for the Smagorinsky constant (C_s) in 3D simulations that are based on finite difference/volume methods employing explicit discretization schemes for unsteady term causing negative numerical diffusion. However, for discritization schemes resulting in small numerical diffusion such as the 2nd order implicit scheme used in the present study, use of rather small value of C_s ($=0.032$) is recommended by recent studies (Oka and Ishihara, 2009; Ma et al., 2000).

2.2. Boundary Conditions near wall

For a finely resolved laminar sublayer, the wall shear stress is obtained from the laminar stress–strain *relationship* as follows:

$$\frac{\bar{u}}{u_\tau} = \frac{\rho u_\tau y}{\mu} \quad (4)$$

But for a mesh unable to resolve laminar sublayer, the centroid of the wall-adjacent cell is assumed to fall within the logarithmic region of boundary layer and the law-of-the-wall is employed:

$$\frac{\bar{u}}{u\tau_\tau} = \frac{1}{k}\ln E\left(\frac{\rho u_\tau y}{\mu}\right) \quad (5)$$

where $\bar{u}$ is the filtered velocity tangential to wall, u_τ is the friction velocity, k (von Kármán constant) is 0.418 and the constant E is 9.793.

2.3. Solution procedure

The governing equations are discretized using finite volume method that uses the integral form of the conservation equations to be solved for the control volumes in computational domain. Central difference scheme for convective terms and the second order implicit scheme for unsteady terms are used. SIMPLEC (SIMPLE-Consistent) algorithm is used to achieve the pressure–velocity decoupling. The scheme used to simulate the moving boundary conditions is explained in the next section.

2.4. Control of mesh motion

Generally Arbitrary Langrangian–Eulerin (ALE) formulation is used to simulate the FSI (Tamura and Itoh, 1997; Nomura and Hughes, 1992). However, in this study, it is aimed to develop a numerical wind tunnel that may include turbulence generator at a later stage. Relative motion between static vortex generators and the oscillating model section will occur that can be simulated using sliding mesh technique. Main idea of using the sliding mesh is to help achieve a numerical wind tunnel that can simulate test conditions similar to the wind tunnel experiments.

In the sliding mesh method, the meeting faces of two neighboring blocks moving relative to each other are associated with each other to form a grid interface. The grids of these blocks

at the interface do not match exactly and grid of one block can have more than one neighboring grids. The estimation of flux across such non-conformal interfaces is required during the computation process. To estimate the flux across the interface, consider two adjoining structured grid blocks that move relative to each other as shown in Fig. 1. During their motion, the intersection of grid blocks at the interface is determined which results in one interior zone where the interface zones overlap (i.e., faces b-c, c-d, d-e, e-f and f-g form an interior zone) and one or more wall zones where they do not (i.e., faces a-b and g-h). To compute the flux across the interface into cell V, newly formed faces c-d and d-e are used to compute the required parameters from cells I and II. For the wall zones, appropriate boundary conditions can be used.

2.5. Geometry and boundary conditions

The geometries used in this study are an elongated rectangular section with aspect ratio of 4 and a box girder section with aspect ratio of 3.82 along with the aerodynamic countermeasures. The computational domain used for both free and unsteady analyses is shown in Fig. 2 where domain is divided into the static and moving zones to simulate the oscillation conditions.

The width and depth of domain are 100D and 60D, respectively where D is the depth of model section (Fig. 2). A block-structured grid is used with coarser mesh in the inlet zone, outlet zone and the domain area far from the section; whereas finer mesh is used for the domain area in the vicinity of the section. A close-up of mesh generated around the rectangular section is shown in Fig. 3.

The corners of rectangular section are smoothened with a roundness ratio (r/D) of 0.01, and small size cells mesh are generated near each edge corner to avoid singularity of the solutions. Such small roundness ratio does not significantly affect the flow characteristics such as Strouhal number (Knisely, 1990). An enlarged view of the geometrical configuration and meshing in vicinity of countermeasures used for the box girder section is shown in Fig. 4. Since section attachments are smaller in size compared to the box girder section, it would require a high mesh resolution to capture the flow accurately. Therefore fine mesh is used only in the region closer to box girder section by using sub-domains near and around the complex geometry of box girder sections, see Fig. 4(d). Within these sub-domains, all quantities substantially vary near the solid boundaries and accuracy is especially important. Therefore, tetrahedral grids are employed to ensure the sufficient number of grids. Use of such sub-domains not only helps to generate reasonable meshing, but also allows use of less number of mesh with sufficient accuracy to speed up the calculation process. The dimensions of model sections and analysis conditions used in this study are summarized in Table 1.

For the unsteady analysis where model sections are subjected to oscillations in the heaving mode, the sliding mesh technique with non-periodic velocity inlet grid interface is employed to allow oscillations. The boundary conditions for the wall zones produced from the moving interface zones are set to velocity inlet in order to keep uniformity of flow near outer edges of the simulated domain. Normally the reduced velocities are changed by increasing the wind speed in wind tunnel testing and the effect of change in Reynolds number (R_e) is ignored for sharp edged sections. But in this study, the inflow wind velocity "U" is kept
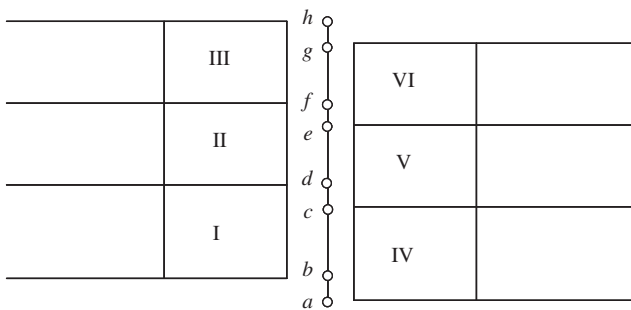

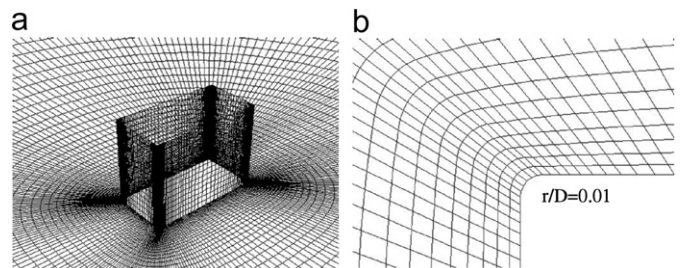
Fig. 1. Interface between adjacent blocks during motion.

Fig. 3. Details of grid near and at the corner of the rectangular section ($B/D=4$): (a) grid near the rectangular section and (b) grid at the corner.
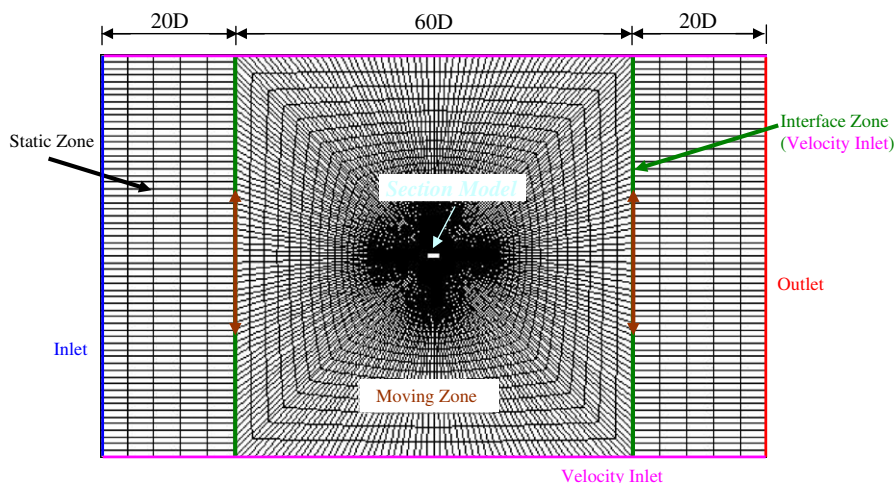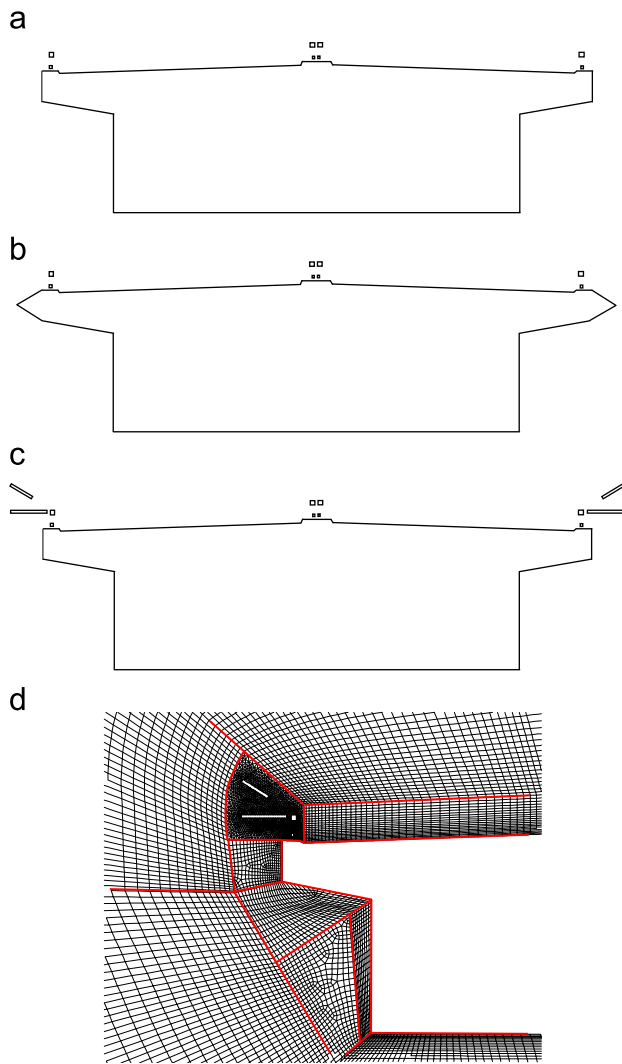

Fig. 2. Overview of computational domain and boundary conditions.

a

b

c

d

Fig. 4. Geometry of box girder section with and without aerodynamic counter-measures: (a) plain section, (b) section with fairings, (c) section with double flaps and (d) meshing scheme on leading edge of the section with double flaps.

Table 1
Dimensions and analysis conditions of the rectangular section and the box girder section.

Parameter	Units	Rectangular section	Box girder section
Width (B)	(m)	0.04	0.0381
Depth (D)	(m)	0.01	0.01
Spanwise length (L)	(m)	0.015	0.01
Aspect ratio (B/D)		4.0	3.81
Reynolds number		1.3×10^4	1.3×10^4
Wind velocity	(m/s)	20	20
Area A ($L \times D$)	(m^2)	0.00015	0.0001
Non-dimensional time step ($\Delta t \times U/D$)		0.04	0.053
Time step (Δt)	(s)	$2.0E-5$	$2.667E-05$

constant for all the cases to avoid any additional phenomenon, if any, arising with change in R_e. Also, throughout unsteady investigations, the angle of attack, that is angle between the direction of width (B) and that of the uniform flow, was kept zero. The maximum turbulence intensity is of the order of 0.001% at the inlet boundary. Symmetry condition is used for top and bottom surfaces of the domain.

2.6. Modeling of oscillating system

To investigate the vortex-induced vibrations, two different techniques will be used to simulate the motion of the model sections under forced and free oscillation conditions. When sections are subjected to forced oscillations, the displacement history is known and is therefore directly imposed. Whereas, when the oscillation results from the vortex shedding, the displacement needs to be computed from the fluid forces acting on the surface of sections.

The forced oscillation of a section is defined by the oscillation frequency (f_o) and the maximum dimensionless amplitude of vibration $A_o = y_{max}/D$, where y_{max} is the maximum amplitude in heaving mode and D is the characteristic length of section, i.e., section depth. A sinusoidal displacement obtained by the relation $A = A_o \sin(2\pi f_o t)$ is explicitly imposed to the section within the fluid domain at each time step before calculating the flow field. The motion remains independent of the fluid field around the section but the wake is strongly affected by the section motion that modifies the forces acting on the model section. The force histories thus obtained are further manipulated to obtain the aeroelastic transfer function for the prediction of vortex-induced vibrations.

On the other hand, vortex-induced vibrations are direct result of the excitation caused by the fluid forces and it requires modeling of fluid–structure interaction. Since vortex-induced vibrations occur in the heaving mode, the structural flexibility can be modeled by using mass–spring system in two dimensions as shown below:

$$m\ddot{x} + c\dot{x} + kx = F(t) \tag{6}$$

where m is the mass, c is the damping, k is the stiffness and $F(t)$ is the time dependent force acting on the model section. The time dependent force on the right hand side of the above equation is obtained by conducting fluid flow analysis around the section. To analyze the structural response of this SDOF system, the equation of motion is integrated using a single-step procedure, namely Runge–Kutta method (Tedesco et al., 1999). A loose sequential approach was used for the fluid structure interaction and coupling algorithm, which is similar to that summarized by Placzek et al. (2008).

3. Performance of numerical model

The investigations on the aeroelastic instability of rectangular section with an aspect ratio of 4 are summarized in this section. First this section investigates the forced oscillation analysis to verify the frequency response component of unsteady lift force and the wake characteristics of rectangular section are examined. Then the free oscillation computations are pursued and the amplitude of vortex-induced vibrations is verified. Finally, for the box girder section, amplitudes under free oscillation conditions in the presence of aerodynamic countermeasures are simulated.

3.1. Unsteady lift force and wake flow velocity

The unsteady lift forces acting on the rectangular section are obtained by performing the forced oscillation simulations at a defined frequency (f_o) and amplitude (A_o). The reduced velocity is changed by changing the frequency of vibration (f_o), whereas the oscillatory amplitude (A_o) is kept constant. An oscillation amplitude of 0.02D is used in this study to be consistent with the experimental conditions of a previous study (Washizu et al., 1978), which is used for comparison purposes.
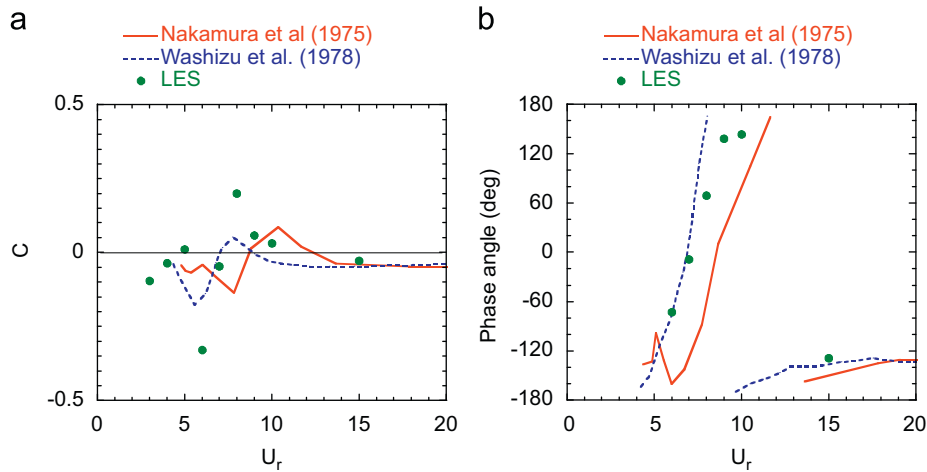
Fig. 5. Unsteady lift force components of rectangular section ($B/D=4$) at an amplitude of 0.02D: (a) Imaginary component of the unsteady lift force and (b) phase angle of the unsteady lift force with the amplitude.

Fig. 5 shows the frequency response characteristic of unsteady lift force acting on the rectangular section when subjected to forced oscillations. The variation of the imaginary part of unsteady lift with increase in the reduced velocity ($U_r = U/fD$) can be seen in Fig. 5(a). This imaginary part of unsteady lift force (C) is related to the flutter derivative h_1^* that represents an aeroelastic transfer function between the wind force and the system displacement. Therefore a close examination of this component of the unsteady lift force enables prediction of the velocity regions where vortex-induced vibration may occur due to negative aerodynamic damping. For the rectangular section, the unsteady lift force component (C) changes from a negative to a positive value at low reduced velocities, and again becomes negative at higher reduced velocities. The positive value of the force component indicates the presence of self-excited vibration caused by the negative aerodynamic damping at reduced velocities ranging from 7 to 9. Also a change in the sign of C (from negative to a positive value) at $U_r=5$ is observed from simulated results that is in accordance with the pattern observed during previous experimental studies (Washizu et al., 1978; Nakamura and Mizota, 1975). In addition, an abrupt change in phase between the lift force and the amplitude of vibration is observed at the reduced velocities that result in negative aerodynamic damping as shown in Fig. 5(b). A good agreement is found between the simulated and experimental results regarding the onset of instability at low reduced velocities.

Fig. 6 shows the variation of phase angle between the wake flow velocity $U_w(t)$ and oscillation amplitude with change in the reduced velocity. The wake flow velocity during forced oscillations is measured at a point P situated at 4.4D downstream the model section and it is kept stationary in order to match the experimental setup. The procedure used to calculate the phase between the amplitude history and wake wind velocity is similar to that used for the unsteady lift force coefficients. An abrupt increase in phase angle at the low reduced velocities, which was observed in a previous experimental study (Nakamura and Mizota, 1975), is well captured.

3.2. Free oscillation response of the rectangular section and the box girder section

The vibration of elastically mounted rectangular section as a result of fluid forcing is a basic case of fluid–structure interactions. The effective structural damping is known to increase with
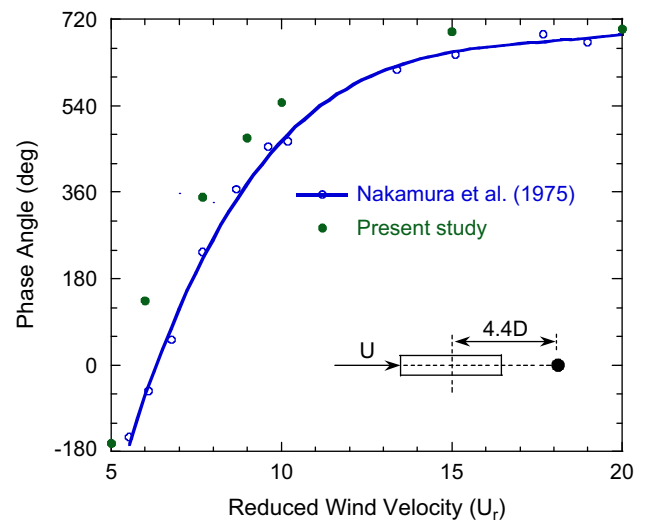

Fig. 6. Phase angle of wake flow velocity for the rectangular section ($B/D=4$).

vibration amplitude but for vortex-induced vibrations, being a self-limiting process, this structural behavior is not taken into account here. A constant Scruton number (S_c) that characterizes the tendency of occurrence of large amplitude of vortex-induced vibrations is used as defined below:

$$S_c = 2\delta_s m_e / \rho d^2 \qquad (7)$$

where δ_s is the logarithmic decrement of structural damping. The total damping of the system thus becomes proportional to the summation of structural and aerodynamic dampings. Therefore in addition to the modeling of fluid flow, an important consideration is the choice of proper Scruton number to accurately simulate the structural response under free oscillation conditions.

To be consistent with the previous experimental studies, the free oscillation simulations for the rectangular section are performed at $S_c=3$. Fig. 7 shows change in dimensionless amplitude with increase in the reduced velocity. A good agreement is found among the simulated amplitude of vibration (η) and that of experimental ones. For comparison purposes, results of κ–ε model (Shimada, 2000) under similar numerical conditions are presented. Though κ–ε model could not simulate the stochastic component of unsteady flow (Shimada and Ishihara, 2002), the amplitude of vortex-induced vibration is predicted reasonably well. However a
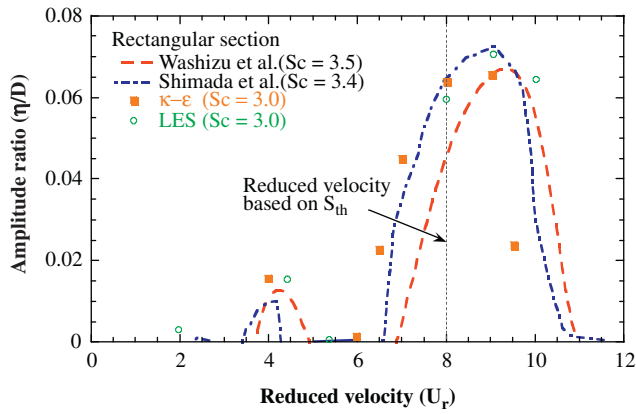
Fig. 7. Non-dimensional amplitudes of free oscillation as a function of reduced velocity.
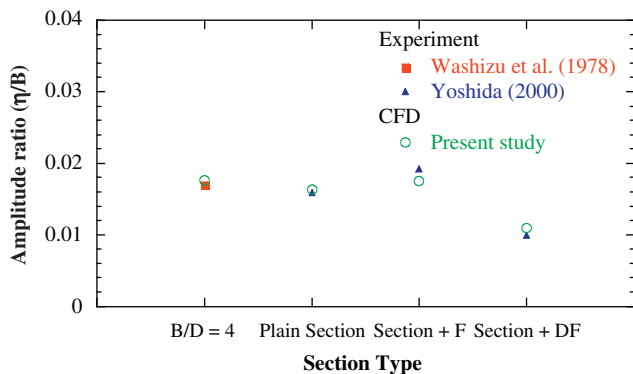

Fig. 8. Comparison of the maximum amplitude ratios for different geometrical configurations.

considerable shift in the reduced velocity corresponding to the maximum amplitude of vibration can be observed.

Next the capability of LES to simulate the flow characteristics around complex geometries, such as box girder section with minor details like hand rails and aerodynamic countermeasures, is examined. The free oscillation computations are performed for box girder section at $S_c = 6$ (Yoshida, 2000). It is interesting to note that the maximum amplitude of box girder section remains similar to that observed in case of rectangular section (Fig. 8). Thus it shows that the geometric modifications done to the basic rectangular section for obtaining the current configuration of box girder section have marginal impact on the amplitude of vibration. Further a reduction in maximum amplitude in the presence of double flaps is predicted well, and the simulated amplitude is found consistent with that of the experimental ones. Whereas adverse effect of fairings leading to rather large amplitude of vortex-induced vibration is well captured by the present study. The mechanism of reduction in the amplitude of the box girder section will be discussed in a later section.

4. Identification of reduced velocity for the maximum amplitude of vibration

The motivation of this section is to assess how a reduced velocity can be identified for predicting the maximum amplitude of vortex-induced vibrations. It is well known that, in wind tunnel experiments, the maximum amplitude is obtained by performing free oscillation experiments over a range of reduced velocities.

However, in case of numerical testing, this method would be very cumbersome and timely expensive. Therefore, it is necessary to develop a method that can predict a reduced velocity resulting in maximum amplitude of vortex-induced vibrations. In this section, first suitability of the Strouhal number to identify the reduced velocity is examined. Then a method for identification of the critical reduced velocity is proposed based on the forced oscillation simulations. Finally the performance of proposed method is evaluated using free oscillation simulations.

A well established wake of a fixed section results in a periodic vortex street whose frequency is regarded as Strouhal frequency (f_s) so that Strouhal number (S_t) becomes $f_s D/U$. Under the free oscillation conditions, large amplitudes of vibration are observed when shedding frequency (f_s) approaches the natural frequency (f_n) of the oscillating system and this synchronization of frequencies is known as "lock-in". This lock-in phenomenon occurs over a range of reduced velocities where the oscillation frequency controls the vortex shedding frequency, i.e., shedding frequency jumps from that of a stationary section to the oscillation frequency. Since vortex-induced vibrations occur over a range of reduced velocities, a reduced velocity leading to the maximum amplitude of vibration is not necessarily the one obtained from Strouhal number, i.e., Strouhal number can only indicate reduced velocity in the vicinity of which vortex-induced vibration would occur. For example, a previous experimental study (Washizu et al., 1978) has shown that Strouhal number for the rectangular section of width to depth equal to 4 is 0.125. The reduced velocity (U_{St}) based on Strouhal number becomes 8.0. Though this velocity (U_{St}) falls within the range of reduced velocities ($6.5 < U_r < 11$), where the rectangular section experiences vortex-induced vibration (Fig. 7), the maximum amplitude of vibration occurs at a reduced velocity higher than U_{St}. This shows that use of Strouhal number does not serve much to identify the reduced velocity resulting in maximum amplitude of vibration.

A method based on the forced oscillation simulations is proposed to identify the reduced velocity resulting in the maximum amplitude of vortex-induced vibrations. Since the power input from the wind in a lock-in range results in the amplitude of vibration, it can be assumed that the higher the power input from the wind, the higher would be the amplitude of vibration. Hence, a reduced velocity corresponds to the maximum power input from the wind, i.e., maximum negative aerodynamic damping is identified as the critical reduced velocity (U_{cr}). Forced oscillation simulations are performed for the box girder section with and without aerodynamic countermeasures to simulate the unsteady force coefficients over a wide range of reduced velocities. The oscillation amplitude is kept constant, i.e., $0.05D$, and only the forced frequency is changed to increase the reduced velocity. The unsteady lift force history is then decomposed using the frequency response analysis to determine the lift force component (C) resulting in negative aerodynamic damping.

Fig. 9 shows the variation of lift component (C) with the reduced velocity for the box girder section with and without aerodynamic countermeasures. For the plain box girder section, only a range of the reduced velocities, i.e., 6.5–8, resulting in negative aerodynamic damping is determined. Later free oscillation simulations will be used in a manner similar to wind tunnel testing to find the maximum amplitude of vibrations. For the box girder section with fairings, the frequency component shows a similar behavior, and a spike is observed for the frequency component (C) that has an amplitude very comparable to the plain box girder section (Fig. 9(b)). However, use of the double flaps has resulted in considerable change in the aerodynamic behavior of the box girder section. The spikes observed in case of plain section and section with fairings have
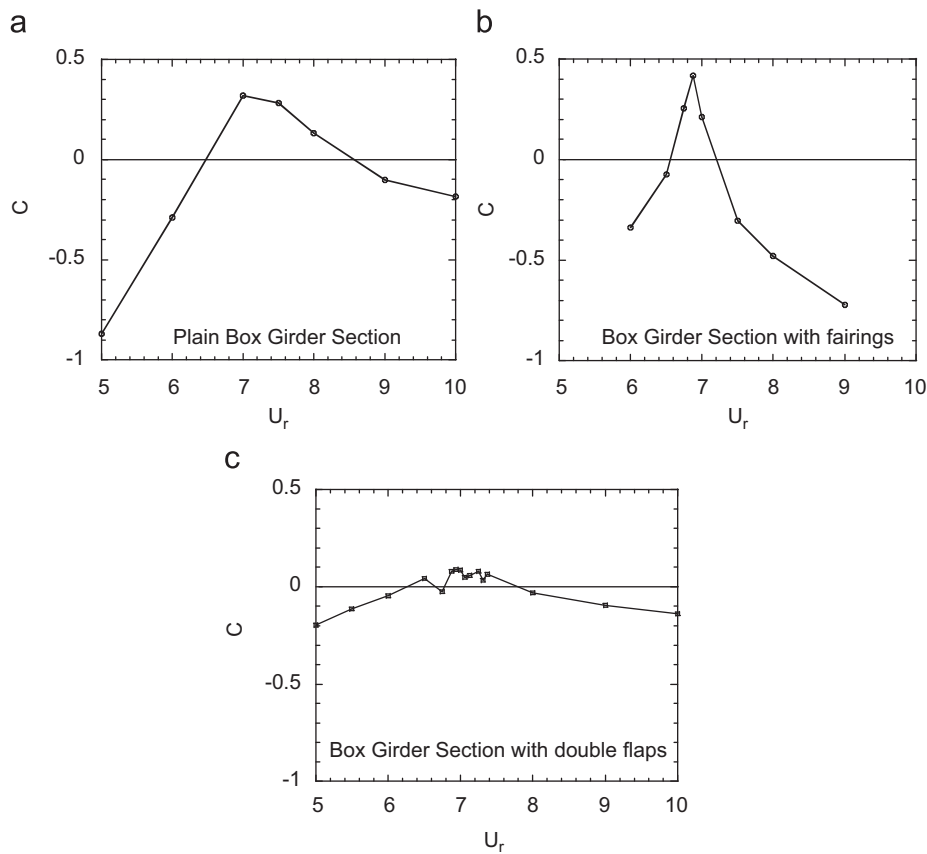
Fig. 9. Variation of the unsteady lift force component with reduced velocity for the box girder section.

disappeared and rather a distribution of small values of the frequency component (*C*) is observed (Fig. 9(c)). Therefore, an intensive investigation is carried out to accurately identify the critical reduced velocity that is found to be 6.935. It can be seen that the introduction of aerodynamic countermeasures has modified the critical reduced velocities too.

To ascertain the efficiency of the proposed method, the free oscillation amplitudes of the box girder sections are simulated and the results are examined against the identified reduced velocities. Fluid—structure interaction (FSI) is employed to simulate the dynamic response of the box girder section under unsteady lift forces caused by the vortex shedding. The structural parameters, for the free oscillation simulations, are chosen such that Scruton number becomes equivalent to that of the wind tunnel experiments (Yoshida, 2000). The free oscillation results are summarized in Fig. 10 for the box girder sections with and without aerodynamic countermeasures. For the plain box girder sections, the maximum amplitude of vibration is observed at $U_r=7.2$ that falls within the identified range of reduced velocities. The amplitudes of vibrations larger than the plain section are observed for the section with fairings and the maximum amplitude of vibration for this configuration occurred at a reduced velocity close to the identified one (Fig. 9(b)). On the other hand, the free oscillation simulation of the section with double flaps resulted in maximum amplitude of vibration at a reduced velocity, which is consistent with the previously identified value. Though a small difference can be observed between the identified reduced velocities and those obtained from the free oscillations, the difference in the maximum amplitude of vibration is negligible. It is noteworthy to mention here that the prediction accuracy of proposed method depends upon the velocity interval used during the forced oscillations, i.e., prediction can be improved by performing the forced oscillation
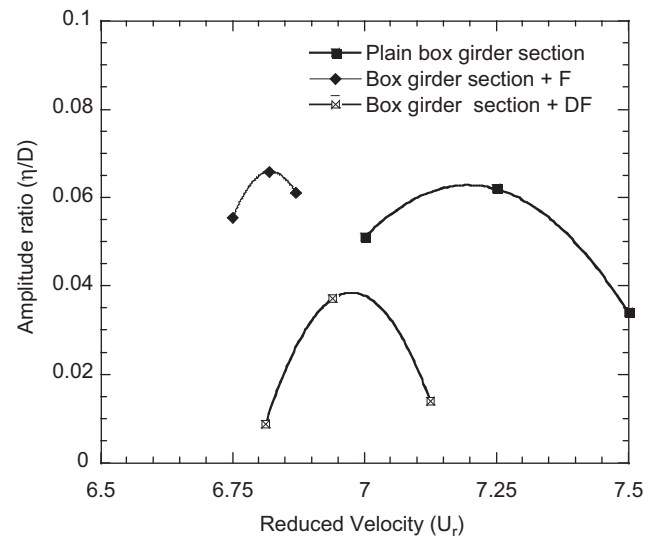

Fig. 10. Variation of non-dimensional amplitude of VIV's with reduced velocity.

simulation at smaller intervals as shown here for the double flaps case.

From comparison of the normalized amplitudes, it is evident that a change in reduced velocity has significant effect on the oscillation amplitudes. Therefore to identify the maximum amplitudes, a large number of free oscillation simulations would be required at small reduced velocity intervals, which makes the whole process computationally expensive because of the large number of cycles required to achieve the established flow

conditions. However the proposed method makes use of the forced oscillation simulation to identify the critical reduced velocity that require only few oscillations to reach the established flow conditions. Therefore use of the proposed method to clearly identify the reduced velocity corresponding to the maximum amplitude of vortex-induced vibration would significantly reduce the computational efforts.

5. Effect of aerodynamic countermeasures

In the previous section, the free oscillation simulations of the box girder sections have clearly shown dependence of the amplitude of vibration on the type of aerodynamic counter-measure used (Fig. 10). Rather large amplitude of vibration is observed for the box girder section with fairings; whereas in the
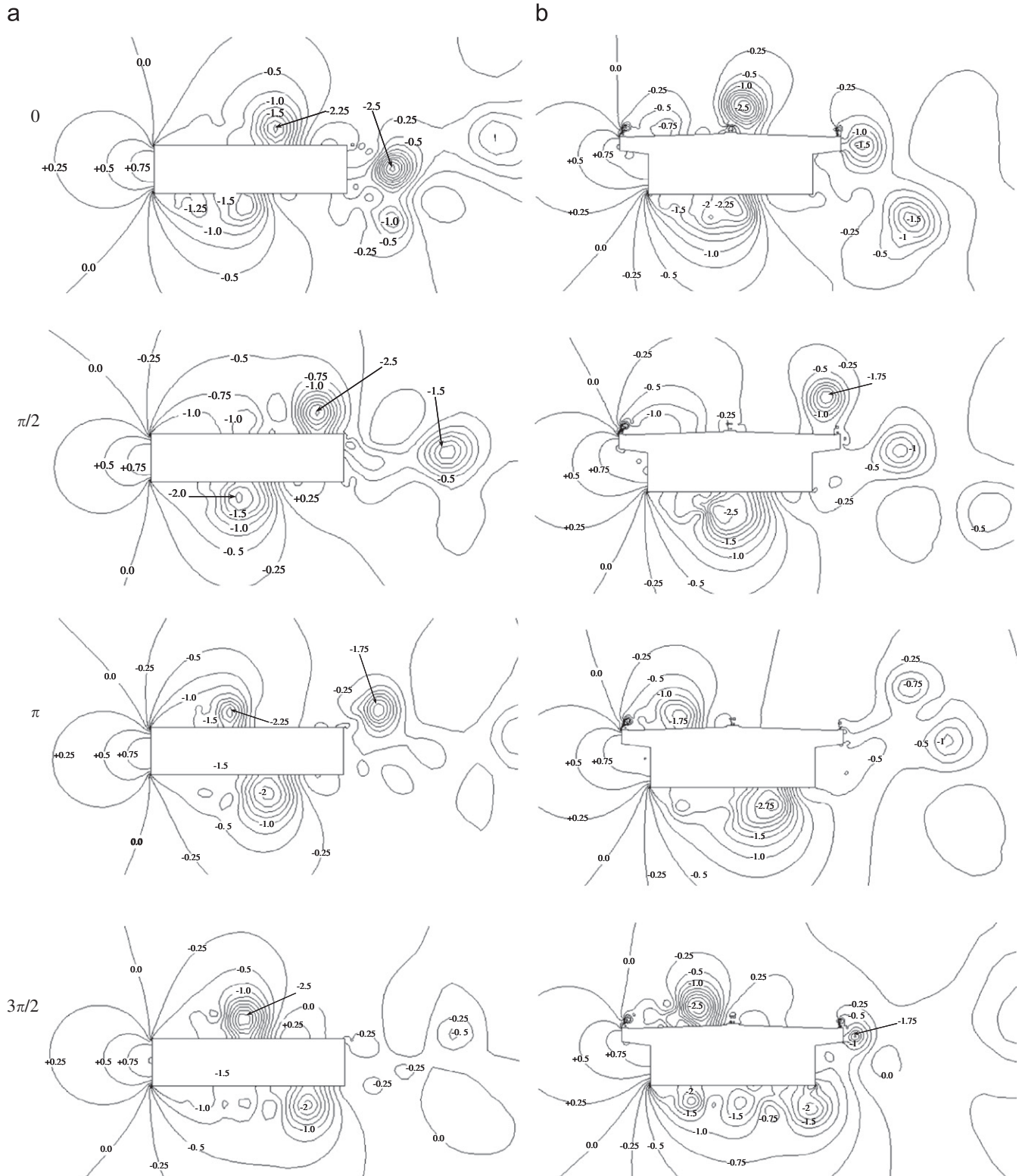

Fig. 11. Pressure distribution around the rectangular section and the box girder section during one cycle.

presence of double flaps, the maximum amplitude of vibration is reduced to half of those observed for the plain box girder section and the section with fairings. This section aims to illustrate and understand the suppression mechanism of aerodynamic counter-measures. First changes in the characteristics of the unsteady lift and then the flow conditions around freely oscillating sections are

pursued to understand the mechanism of reduction in amplitude of vibration by such countermeasures.

Forced oscillation time histories of the unsteady lift are now very important data, because during lock-in, the wake conditions are also controlled by the oscillation of section. It is interesting to note that the characteristics of the unsteady lift force remain
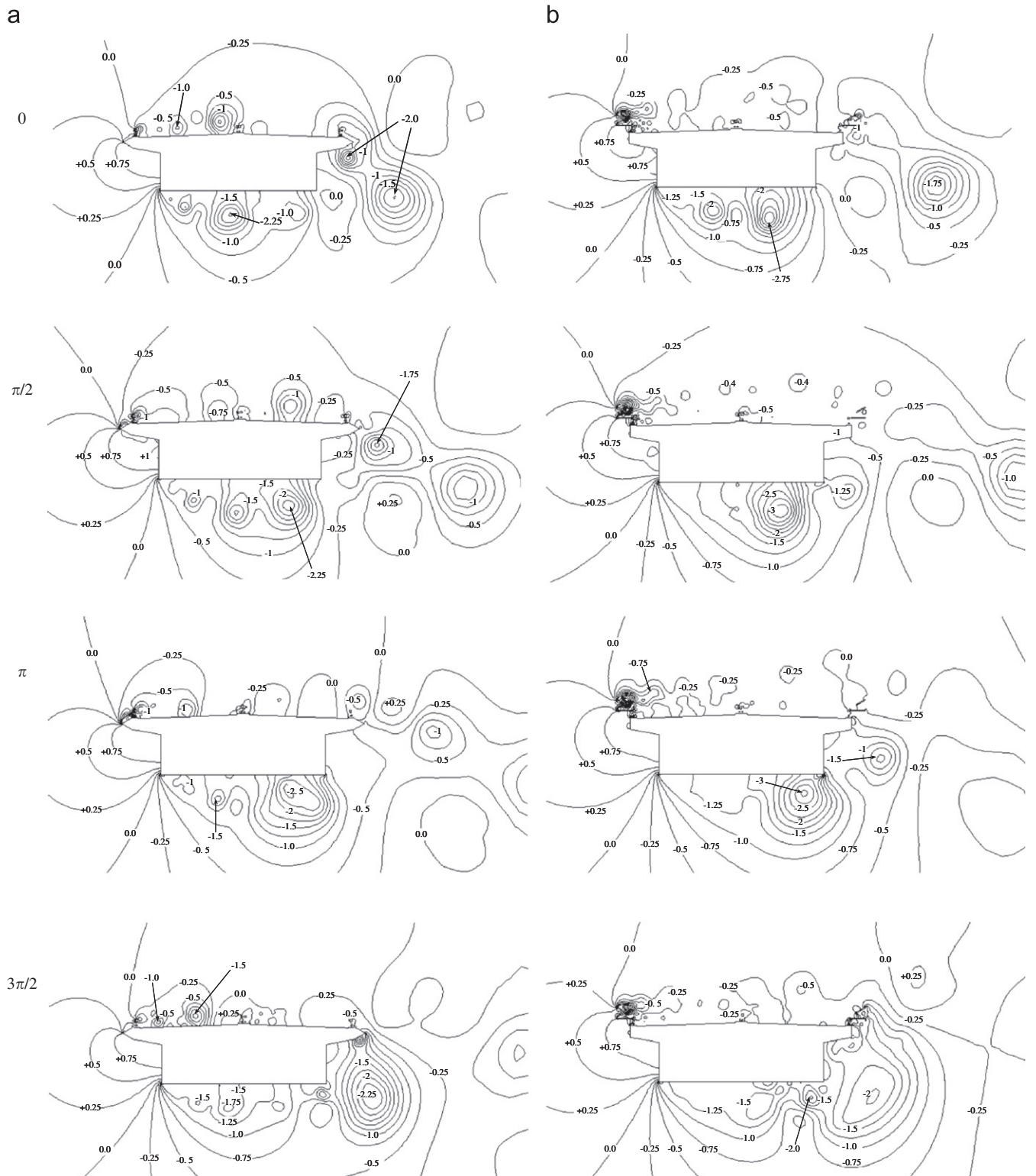

Fig. 12. Distribution around the box girder section with aerodynamic countermeasures during one cycle.

similar despite the modifications done to the generic rectangular section for obtaining the current configuration of the box girder section (see Fig. 5(a) and Fig. 9(a)). Though a deviation in Strouhal number is observed, the characteristics of the lift force component (C) in the region of negative aerodynamic damping remain similar, i.e., a gradual increase from negative to positive values and vice versa. Similarly, in the presence of fairings, the lift force component clearly shows an intensified negative damping at the critical reduced velocity (Fig. 9(b)). But the region of negative aerodynamic damping becomes much narrower compared to that of the plain section. On the other hand, introduction of double flaps to the box girder section has changed the characteristics of the unsteady lift significantly. The range of reduced velocity resulting in negative aerodynamic damping is comparable to that of the plain section, but previously observed peak has diminished (Fig. 9(c)). The reduced amplitude of the lift force component (C) indicates smaller negative aerodynamic damping that results in small oscillation amplitude in the presence of double flaps. These changes in the characteristics of the unsteady lift indicate that the flow around the bridge section is significantly altered by the introduction of aerodynamic countermeasures.

Now pressure contours and velocity vectors are examined to clarify the changes in the flow conditions around the box girder sections by the aerodynamic countermeasures. The pressure is normalized to a dimensionless coefficient (c_p) as shown below:

$$c_p = \frac{P - P_{ref}}{1/2 \, \rho U^2} \tag{8}$$

where P is the pressure near the section, P_{ref} is the pressure at far reference point, which is the lower corner of velocity inlet, ρ is air density and U is the inflow velocity. Fig. 11 shows the instantaneous pressure contours around the rectangular and the box girder sections during one cycle of oscillation. The visualization of flow around the rectangular section shows that vortex keeps growing during the half cycle from one extreme position to the other one, and travels to rear edge resulting in wake vortex shedding on the way back to the original extreme position. Also, it can be seen that at the time negative pressure concentrates on the upper surface leading to vortex formation, vortex on lower edge departs to the wake that results into relatively large pressure acting on the lower surface. As a result, section is subjected to an upward lift that is in accordance with the upward motion of the section and vice versa. This interaction between the lift force and the section movement is repeated in each oscillation. Therefore, it can be concluded that the section is subjected to an exciting force whose frequency is equal to that of the oscillating section. This simulated behavior agrees with the explanation given by Komatsu and Kobayashi (1980) based on the experimental results.

Similarly alternate vortex shedding from upper and lower surfaces of the plain box girder section can be observed in Fig. 11(b). In addition to the small vortices behind the hand rails, the formation of large vortex on the upper section can be seen that travels in due course of oscillation towards the leeward edge. On the other hand, the flow separation on the lower windward edge is evident that results in formation of vortex on lower surface and travels to the rear end. This alternate vortex shedding applies an oscillating force on the box girder section that results in large amplitude of vibrations in the lock-in region.

The instantaneous pressure contours around box girder section with aerodynamic countermeasures during one cycle at the respective critical reduced velocities are shown in Fig. 12. In case of the box girder section with fairings, the vortices are formed on upper and lower surfaces that travel down to the trailing edge, and these vortices are shed alternatively as observed in the case of plain section. In addition, it is observed that the

wind velocity at the upper leading edge of box girder section increases in the presence of fairings (Fig. 13(b)), and it intensifies the shear layer resulting in the formation of a strong vortex. This strong vortex is responsible for the large negative aerodynamic damping observed during the forced oscillation computations. Therefore use of fairings results in oscillation amplitude that is larger than that of the plain box girder section.

On the other hand, in case of the box girder section with double flaps, vortex formation on the lower edge remains
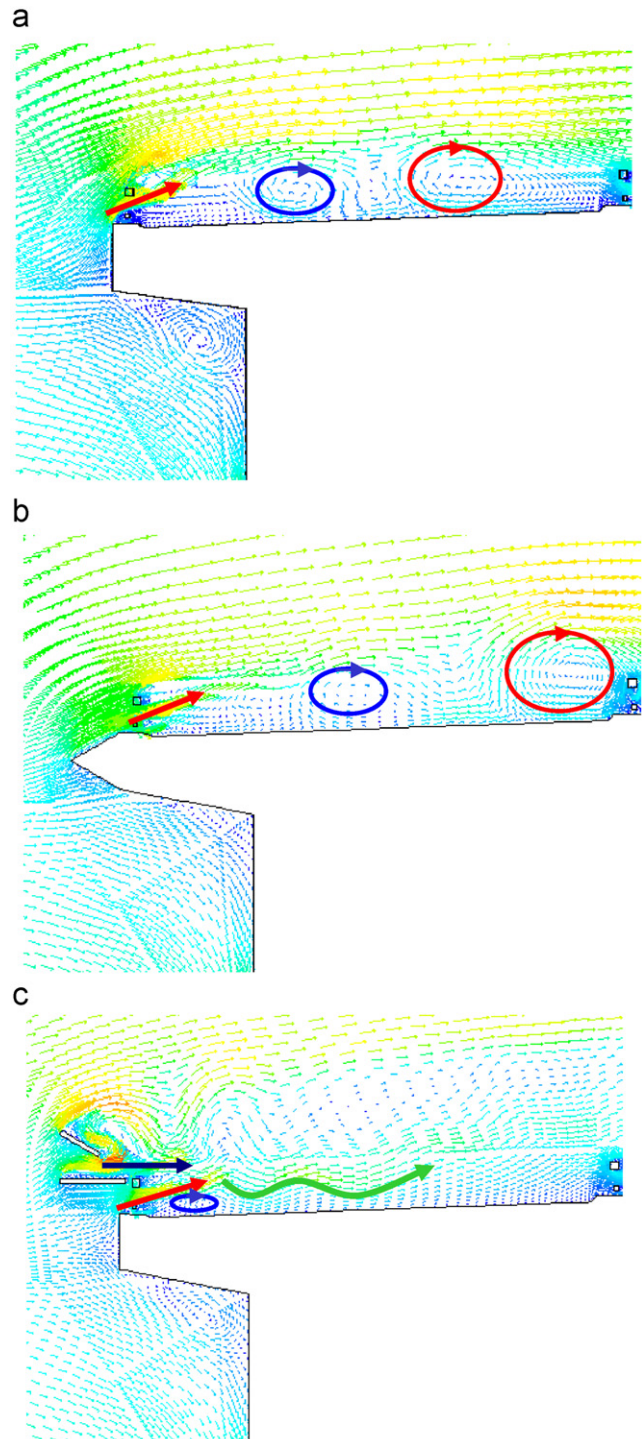

Fig. 13. Instantaneous velocity vectors on the windward side of box girder section at $\eta = 0$ and $U_r = U_{cr}$: (a) plain box girder section, (b) box girder section with fairings and (c) box girder section with double flaps.

undisturbed. However, the strong vortex formation on upper surface disappears and only small vortices behind the double flaps are observed as shown in Fig. 12. It becomes clear from Fig. 13(c) that double flaps have redirected the separated flow towards the upper surface, which results in energization of the shear layer. This energization of the shear layer eliminates formation of vortex on the upper surface and results in small negative aerodynamic damping as observed from the forced oscillations results. Therefore the use of double flaps resulted in rather small oscillatory force acting on the box girder section, which leads to reduced amplitude of vibration.

6. Conclusions

This paper aims to discuss the reliability of 3D LES turbulence model for the prediction of vortex-induced vibrations of a box girder section in the presence of aerodynamic countermeasures. First the aeroelastic instability of a rectangular section with an aspect ratio of 4 is investigated in a heaving mode. Then the vortex-induced vibrations and the mechanism of reduction in the oscillation amplitude of a box girder section in the presence of aerodynamic countermeasures are clarified.

The suitability of the 3D LES model for modeling the fluid–structure interaction has been demonstrated for the rectangular section. The characteristics of the unsteady lift force acting on the rectangular section and the wake flow conditions are predicted well. The simulated amplitudes of the rectangular section under free oscillation conditions agreed well with the experimental results. In addition, the changes in the oscillation amplitudes in the presence of different aerodynamic countermeasures are successfully simulated and are found in good agreement with the experimental results. From forced oscillation computations, the aerodynamic countermeasures are found to have drastically altered the aerodynamic characteristics of the box girder section. Introduction of double flaps resulted in small negative aerodynamic damping, which is responsible for smaller amplitude of the vortex-induced vibrations. Furthermore, change in a reduced velocity leading to the maximum amplitude of vibration is observed for these aerodynamic countermeasures. Flow visualization and pressure distribution have shown that use of double flaps resulted in energization of the shear layer formed at the leading edge of the section and diminished the vortex formation on upper surface. However, use of fairings resulted in a strong vortex formation on the upper surface that leads to rather larger amplitude of vibration. Finally, a method to identify the reduced velocity based on forced oscillations is proposed and successfully verified by the free oscillation simulations. Proposed method reduces the computational efforts making the whole process of predicting the maximum amplitude more efficient and economical.

References

Bruno, L., Khris, S., 2003. The validity of 2D numerical simulations of vertical structures around a bridge deck. Mathematical and Computer Modeling 37, 795–828.

Frandsen, J.B., 1999. Computational fluid–structure interaction applied to long-span bridge design. Ph.D. Thesis. University of Cambridge.

Frandsen, J.B., 2004. Numerical bridge deck studies using finite elements. Part I: flutter. Journal of Fluids and Structures 19, 171–191.

Fujino, Y., Yoshida, Y., 2002. Wind-induced vibration and control of Trans-Tokyo Bay Crossing Bridge. Journal of of Structural Engineering 128, 1012–1025.

Fujino, Y., 2003. Wind resistant design of bridges–code practice and recent developments. Structural Engineering Series 12, JSCE.

Knisely, C.W., 1990. Strouhal numbers of rectangular cylinder—a review and new data. Journal of Fluids and Structures 4, 371–393.

Komatsu, S., Kobayashi, H., 1980. Vortex-induced oscillation of bluff cylinders. Journal of Wind Energy and Industrial Aerodynamics 6, 335–362.

Larsen, A., 2006. Computation of aerodynamic derivatives by various CFD techniques. In: The Fourth International Symposium on Computational Wind Engineering, Yokohama, Japan. pp.287–290.

Larsen, A., Walther, J.H., 1998. Discrete vortex simulation of flow around five generic bridge deck sections. Journal of Wind Energy and Industrial Aerodynamics 77–78 (1), 591–602.

Larsen, A., Esdahl, S., Andersen, J.E., Vejrum, T., 2000. Storebælt suspension bridge—vortex shedding excitation and mitigation by guide vanes. Journal of Wind Energy and Industrial Aerodynamics 88, 283–296.

Lee, S., Lee, J.S., Kim, J.D., 1997. Prediction of vortex-induced wind loading on long-span bridges. Journal of Wind Energy and Industrial Aerodynamics 67–68, 267–278.

Ma, X., Karamanos, G.S., Karniadakis, G.E., 2000. Dynamics and low-dimensionality of a turbulent near wake. Journal of Fluid Mechanics 410, 29–65.

Matsumoto, M., Niihara, Y., Kobayashi, Y., 1994. On the mechanism of flutter phenomena for structural sections. Journal of Structural Engineering 40A, 1019–1024 in Japanese.

Matsumoto, M., 1996. Aerodynamic damping of sections. Journal of Wind Energy and Industrial Aerodynamics 59, 159–179.

Matsumoto, M., Kobayashi, Y., Shirato, H., 1996. The influence of aerodynamic derivatives on flutter. Journal of Wind Energy and Industrial Aerodynamics 60, 227–239.

Morgenthal, G., 2000. Comparison of numerical methods for bridge-deck aerodynamics. M.Phil. Thesis. University of Cambridge.

Morgenthal, G., 2005. Advances in numerical bridge aerodynamics and recent applications. Structural Engineering International Reports, 95–100.

Nakamura, Y., Mizota, T., 1975. Unsteady lifts and wakes of oscillating rectangular sections. Journal of the Engineering Mechanics Division, 871–885.

Nomura, T., Hughes, T.J.R., 1992. An arbitrary Lagrangian–Eulerian finite element method for interaction of fluid and a rigid body. Computer Methods in Applied Mechanics and Engineering 95, 115–138.

Oka, S., Ishihara, T., 2009. Numerical study of aerodynamic characteristics of a square prism in a uniform flow. Journal of Wind Energy and Industrial Aerodynamics 97 (11–12), 548–559.

Owena, J.S., Hargreavesa, D.M., 2007. Bridge deck aero-elasticity: comparisons of computational models with wind tunnel tests. In: ICWE12, Cairns, Australia. pp. 151–158.

Placzek, A., Sigrist, R., Hamdouni, A., 2008. Numerical simulation of an oscillating cylinder in cross-flow at low Reynolds number: forced and free oscillations. Computer and Fluids. doi:10.1016/j.compfluid.2008.01.007.

Sarwar, M.W., Ishihara, T., Shimada, K., Yamasaki, Y., Ikeda, T., 2008. Prediction of aerodynamic characteristics of box girder bridge section using LES turbulence model. Journal of Wind Energy and Industrial Aerodynamics 96 (10-11), 1895–1911.

Shimada, K., Ishihara, T., 1999. Prediction of aeroelastic vibration of rectangular cylinders by κ–ε model. Journal of Aerospace Engineering 12 (4), 122–135.

Shimada, K., Ishihara, T., 2002. Application of a modified K-ϵ model to the prediction of aerodynamic characteristics of rectangular cross-section cylinders. Journal of Fluids and Structures 16 (4), 465–485.

Shimada, K., 2000. A study on evaluation of aerodynamic characteristics and prediction of aeroelastic vibrations of rectangular cylinders by κ–ε model. Ph.D. Thesis. Kyoto University, Japan.

Smagorinsky, U., 1963. General circulation experiments with the primitive equations, Part I: the basic experiment. Monthly Weather Review 91, 99–164.

Tamura, T., Itoh, Y., 1997. Three-dimensional vortical flows around a bluff cylinder in unstable oscillations. Journal of Wind Energy and Industrial Aerodynamics 67&68, 141–154.

Tamura, T., 1999. Reliability on CFD estimation for wind–structure interaction problems. Journal of Wind Energy and Industrial Aerodynamics 81, 117–143.

Taylor, I.J., Vezza, M., 1999. Analysis of the wind loading on bridge-deck sections using a discrete vortex method. In: Larsen, A. (Ed.), Wind Engineering into the 21st Century. Balkema, Rotterdam, pp. 1345–1352.

Taylor, I.J., Vezza, M., 2009. A numerical investigation into the aerodynamic characteristics and aeroelastic stability of a footbridge. Journal of Fluids and Structures 25 (1), 155–177.

Tedesco, J.W., McDougal, W.G., Ross, C.A., 1999. Structural Dynamics: Theory and applications. Addison-Wesley.

Washizu, K., Ohya, A., Otsuki, Y., Fuji, K., 1978. Aeroelastic instability of rectangular cylinders in a heaving mode. Journal of Sound and Vibration 59 (2), 195–210.

Yoshida, Y., 2000. A study about the vortex induced vibration and control of a continuous steel box girder bridge. Ph.D. Thesis. The University of Tokyo.